Electronic Supplementary Material (ESI) for New Journal of Chemistry.

Electronic Supporting Information

Simple and Modular Design Platform of Bimodal

Turn-On Chemodosimeters for Oxophilic Metal Cations

David T. Hogan and Todd C. Sutherland*

2500 University Drive NW

Calgary, AB, Canada

T2N 1N4

Email at: todd.sutherland@ucalgary.ca

Contents

Section 1 General Considerations

Acetonitrile (Sigma-Aldrich, 99.93+% for HPLC) for all solutions was dried by cycling 3 × over flame-dried 3 Å molecular sieves under N_2, each cycle lasting at least 24 h. It was kept under N_2 prior to use and filtered with Pall Microdisc 0.2 μm PTFE membranes to remove sieve dust. The metal chloride salts were obtained and treated in the following ways: $AlCl_3$ (Sigma, Aldrich, anhydrous powder, 99.999% trace metals basis). $InCl_3$ (Sigma-Aldrich, anhydrous powder, 99.999%) and NaCl (Fisher Scientific, 99.9%) were flamed under vacuum for 5 minutes. $ZnCl_2$ (Sigma Aldrich, anhydrous, 99.99%), LiCl (Sigma-Aldrich, 99.9%) and TBACl (Sigma-Aldrich, ≥ 97%) were melted by flame under vacuum and allowed to re-solidify under N_2. All above metal chloride salts were stored in a vacuum desiccator under indicating Drierite prior to use. $N(CH_3)_4OH$ (Sigma-Aldrich, pentahydrate, 99%) was used as received.

Solutions of **X=NCH$_3$**, **X=O** and **X=S** and all metal chloride salts were prepared in volumetric flasks which had been pre-flushed with N_2 for at least 5 minutes and further handled under a blanket of N_2. After use, the headspace was flushed with N_2 for at least 30 seconds and the flask was sealed with Parafilm.

Electronic absorption spectroscopy was performed using a Varian Cary 5000 UV-visible-NIR spectrophotometer in dual beam mode. Solutions were measured in dried CH_3CN at 298 K, referenced against blank dried CH_3CN in quartz 10 mm path length cuvettes with elongated necks. The UV lamp-changeover was switched to 310 nm instead of 350 nm. The solutions were prepared under a blanket of N_2 and stoppered with a rubber septum to maintain inert atmosphere. When titrating, a small aliquot (several μL) was added through the septum into the cuvette containing $2\times10^{-5-}$ M chemodosimeter in 2 mL CH_3CN with a small magnetic stir bar and stirred for 30 seconds before measurement.

Fluorescence spectroscopy was performed using a Jasco FP-6600 on medium sensitivity mode collecting a single scan. The excitation bandwidth was 1 nm, emission bandwidth of 6 nm, integration time of 2 seconds, data pitch of 1 nm, scanning speed of 200 nm/minute. The same solution preparation and titration protocols were performed as above.

An initial metal cation screening of **X=NCH$_3$**, **X=O** and **X=S** in various polar solvents revealed that the chemodosimeters were intolerant of water for two distinct reasons. The products of dehydroxylation, **[X=O]$^+$** and **[X=S]$^+$**, were too electrophilic and were likely converted back to the masked tertiary alcohols by residual water such that no chemodosimetric behaviour was observed. Conversely, the acridinium **[X=NCH$_3$]$^+$** was stable enough in wet solvents that it would spontaneously form over a few hours, even in the absence of metal cations, giving a false positive signal. With this information in-hand, metal cation screening was conducted in CH_3CN because both initial and final species were freely soluble and CH_3CN can be rigorously dried. Judicious choice of the metal cations was also necessary for the following reasons: A) solubility limitations (Sr^{2+}, Ba^{2+}, Mg^{2+}, Ca^{2+}, Zr^{4+}, Cd^{2+}, Hg^{2+}, $Pb^{2/4+}$, Ce^{3+}, Rh^{3+}, Tb^{3+}, Eu^{3+}); B) transition metals that were coloured or formed coloured complexes in CH_3CN were excluded (Cr^{3+}, Ni^{2+}, Ru^{3+}, Pt^{2+}, Pd^{2+}, $Co^{2+/3+}$ and $V^{2/3/4/5+}$); C) metals that exhibited redox behaviour with the chemodosimeters were also excluded ($Fe^{2+/3+}$, Ag^+, Sn^{2+} and $Cu^{1+/2+}$). For these reasons, Na^+, Al^{3+}, Li^+, Zn^{2+} and In^{3+} were chosen for screening.

Section 2 Photographs of Metal Cation Screenings

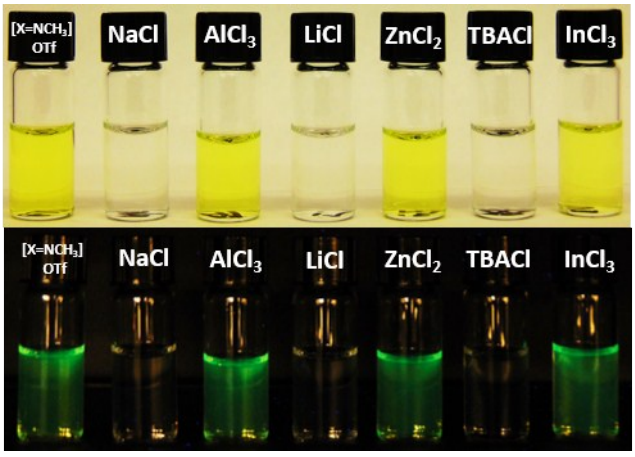

Figure S1. Photograph of *c*. 0.1 mM **X=NCH$_3$** in CH_3CN with a saturating amount of metals, as labelled, under ambient light (top) and 365 nm UV light (bottom). The left-most vial contains **[X=NCH$_3$]OTf** for reference.

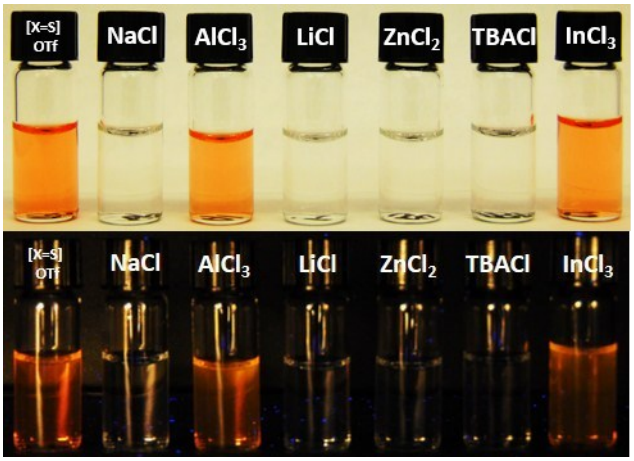

Figure S2. Photograph of *c*. 0.1 mM **X=S** in CH_3CN with a saturating amount of metals, as labelled, under ambient light (top) and 365 nm UV light (bottom). The left-most vial contains **[X=S]OTf** for reference.

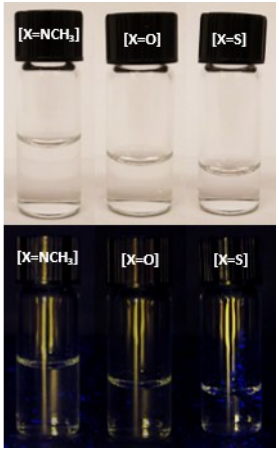

Figure S3. Photograph of *c*. 0.1 mM **X=NCH$_3$** (left), **X=O** (middle), and **X=S** (right) in CH_3CN without added metals, under ambient light (top) and 365 nm UV light (bottom).

Section 3 UV-visible Spectroscopy of **X=NCH$_3$**, **X=O**, **X=S** and **[X=NCH$_3$]OTf**, **[X=O]OTf**, **[X=S]OTf**

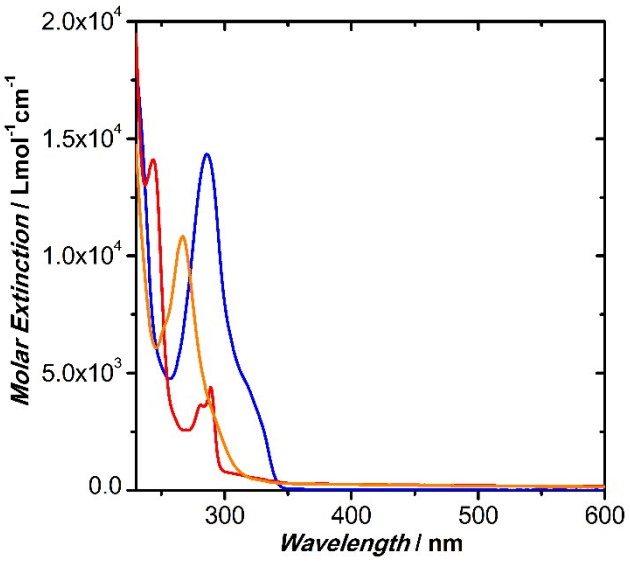

Figure S4. UV-visible spectra of **X=NCH$_3$** (blue), **X=O** (red) and **X=S** (orange) in CH_3CN.

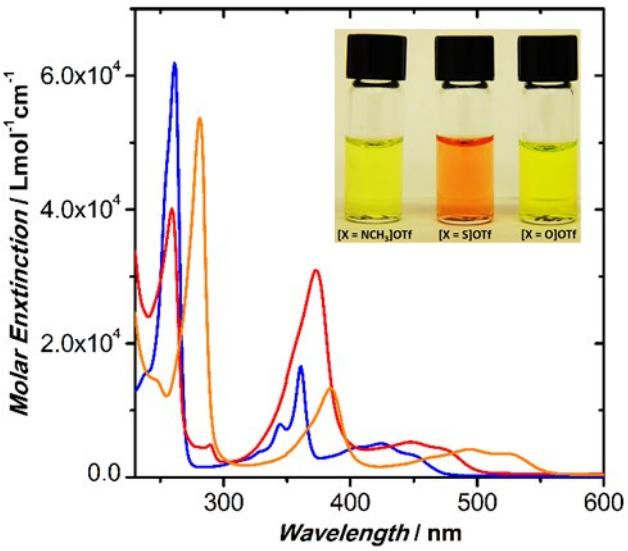

Figure S5. UV-visible spectra of **[X=NCH$_3$]OTf** (blue), **[X=O]OTf** (red) and **[X=S]OTf** (orange) in CH_3CN. Inset: photograph of *c.* 0.1 mM solutions of these compounds under ambient light.

Table S1. Absorption Band Data

	λ_{abs} (nm) / [ε] (L·mol^{-1}·cm^{-1})
X=NCH$_3$	286 [14 000]
X=O	244 [14 000] 289 [4 400]
X=S	267 [11 000]
[X=NCH$_3$]OTf	261 [62 000] 361 [17 000] 424 [5 100]
[X=O]OTf	259 [40 000] 373 [31 000] 447 [5 300]
[X=S]OTf	281 [54 000] 384 [13 000] 493 [4 200]

Section 4 Excitation and Emission Spectroscopy of **X=NCH$_3$, X=O, X=S** and **[X=NCH$_3$]OTf, [X=O]OTf, [X=S]OTf**

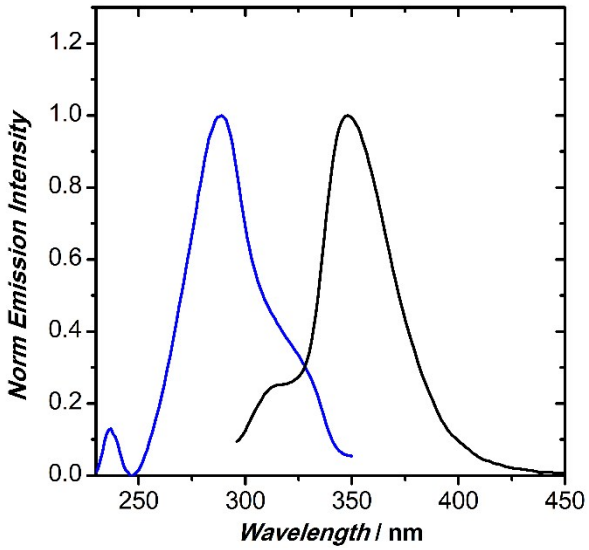

Figure S6. Normalized excitation (blue) and emission spectra (black) of **X=NCH$_3$**. Excitation wavelength: 286 nm.

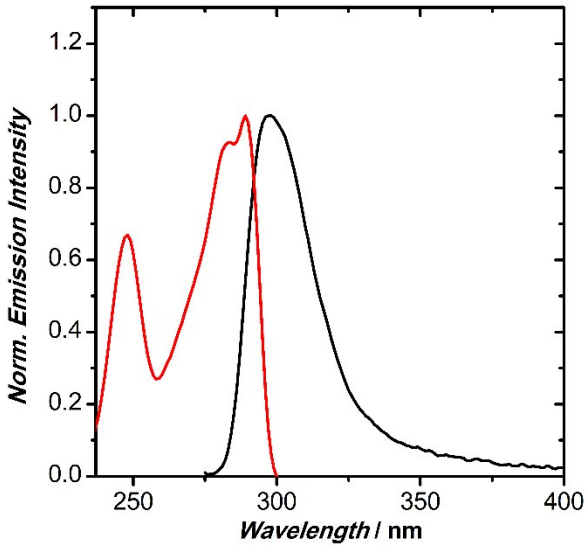

Figure S7. Normalized excitation (red) and emission spectra (black) of **X=O**. Excitation wavelength: 244 nm.

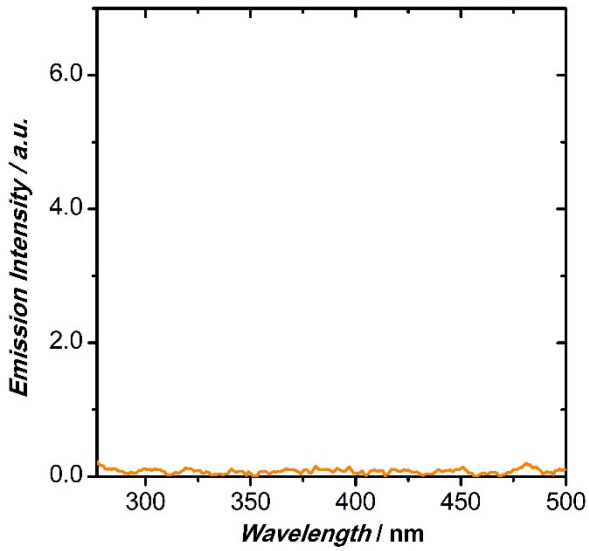

Figure S8. Emission spectrum of **X=S**, exciting at 267 nm.

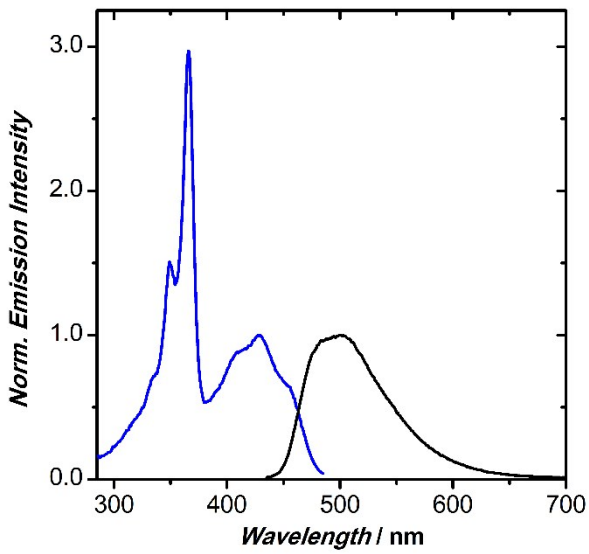

Figure S9. Normalized excitation (blue) and emission spectra (black) of **[X=NCH$_3$]OTf**. Both traces are normalized to the excitation wavelength of 424 nm.

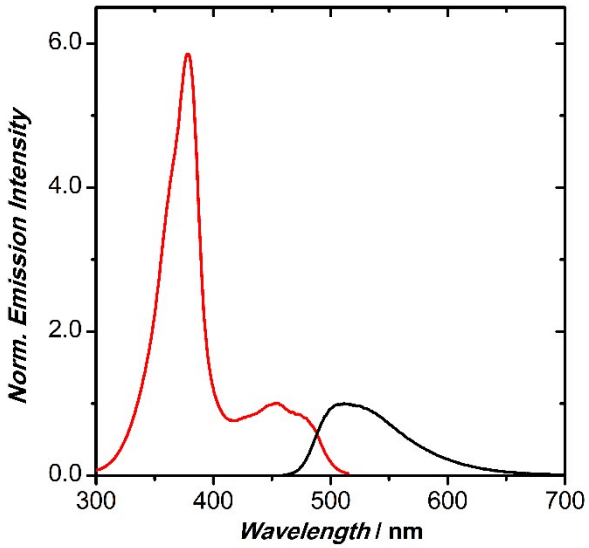

Figure S10. Normalized excitation (red) and emission spectra (black) of **[X=O]OTf**. Both traces are normalized to the excitation wavelength of 447 nm.

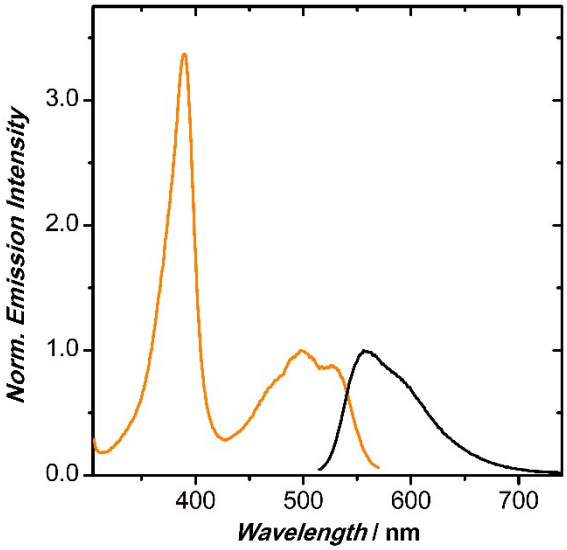

Figure S11. Normalized excitation (orange) and emission spectra (black) of **[X=S]OTf**. Both traces are normalized to the excitation wavelength of 493 nm.

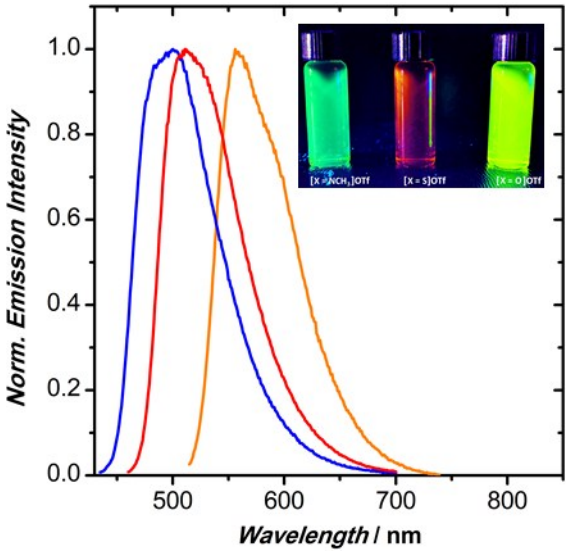

Figure S12. Normalized emission spectra of **[X=NCH$_3$]OTf** (blue, 424 nm excitation), **[X=O]OTf** (red, 447 nm excitation) and **[X=S]OTf** (orange, 493 nm excitation) in CH_3CN. Inset: photograph of *c*. 0.1 mM solutions of these compounds under 365 nm UV light.

Table S2. Emission Data

	λ_{em} (nm)	λ_{exc} (nm)	Relative φ_f
X=NCH$_3$	348	270	0.05 ± 0.01[a]
X=O	298	270	0.11 ±0.01[a]
X=S	—	—	—
[X=NCH$_3$]OTf	500	424	0.05 ± 0.01[b]
[X=O]OTf	513	440	0.63 ± 0.06[b]
[X=S]OTf	563	475	0.05 ± 0.01[c]

[a] Measured against L-tryptophan in pH 7.0 phosphate-buffered water (φ_f = 0.12)
[b] Measured against coumarin 6 in absolute ethanol (φ_f = 0.78)
[c] Measured against rhodamine 6G in Milli-Q water (φ_f = 0.95)

Section 5 UV-visible Spectroscopic Titrations with Metal Cations

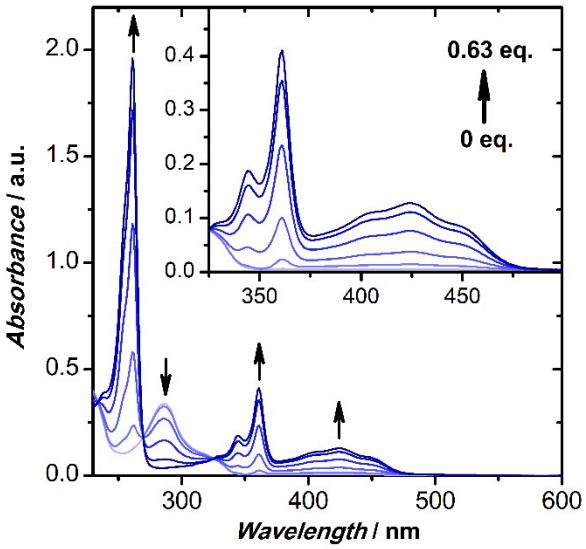

Figure S13a. UV-visible Al^{3+} titration into **X=NCH$_3$**. Initial spectrum in light blue; final spectrum in dark blue.

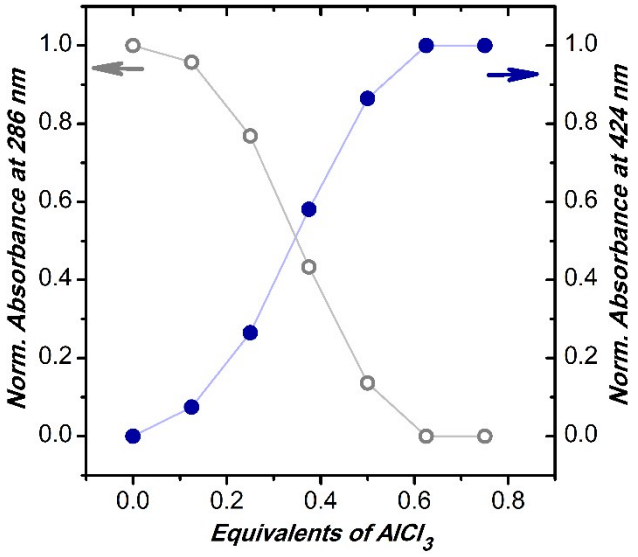

Figure S13b. Normalized absorbance for **X=NCH$_3$** (grey, open) and **[X=NCH$_3$]$^+$** (blue, closed) as a function of titrated equivalents of Al^{3+}.

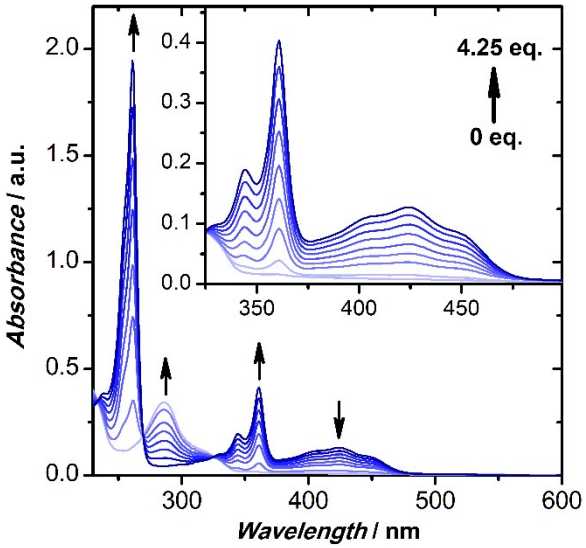

Figure S14a. UV-visible In^{3+} titration into **X=NCH$_3$**. Initial spectrum in light blue; final spectrum in dark blue.

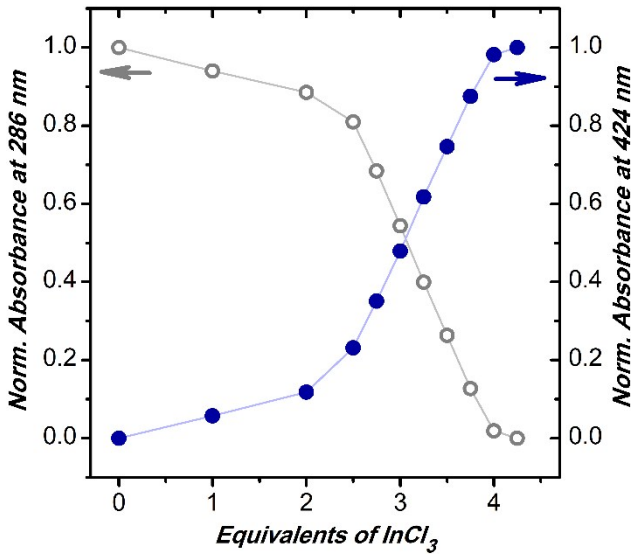

Figure S14b. Normalized absorbance for **X=NCH$_3$** (grey, open) and **[X=NCH$_3$]$^+$** (blue, closed) as a function of titrated equivalents of In^{3+}.

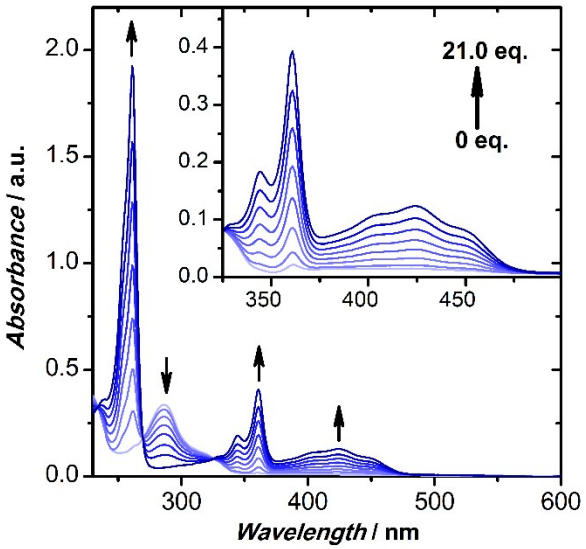

Figure S15a. UV-visible Zn^{2+} titration into **X=NCH$_3$**. Initial spectrum in light blue; final spectrum in dark blue.

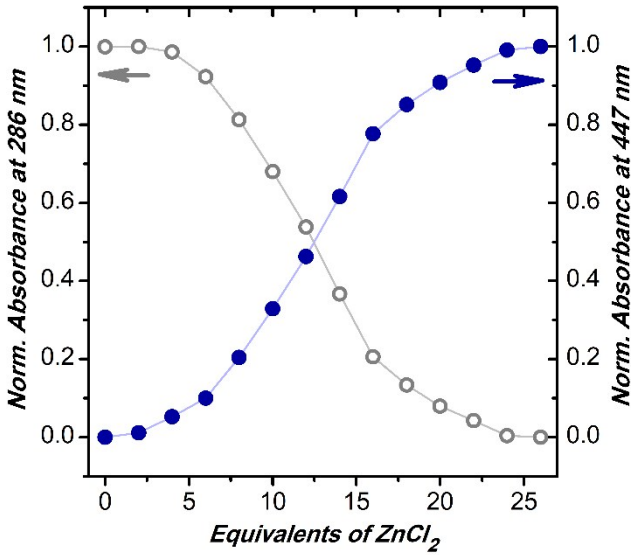

Figure S15b. Normalized absorbance for **X=NCH$_3$** (grey, open) and **[X=NCH$_3$]$^+$** (blue, closed) as a function of titrated equivalents of Zn^{2+}.

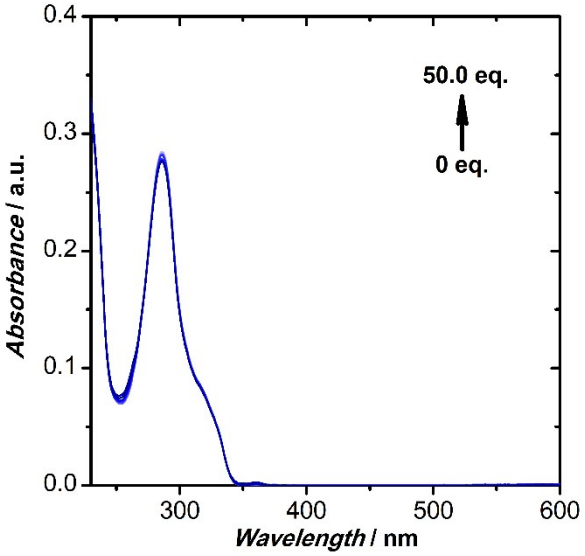

Figure S16. UV-visible Li^+ titration into **X=NCH$_3$**. Initial spectrum in light blue; final spectrum in dark blue.

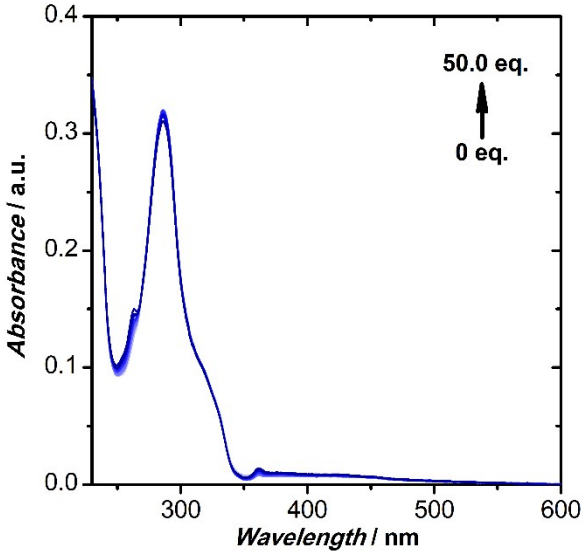

Figure S17. UV-visible Na^+ titration into **X=NCH$_3$**. Initial spectrum in light blue; final spectrum in dark blue.

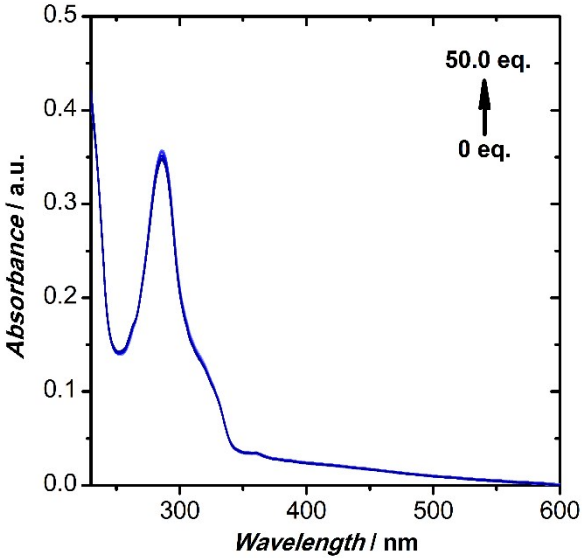

Figure S18. UV-visible TBACl titration into **X=NCH$_3$**. Initial spectrum in light blue; final spectrum in dark blue.

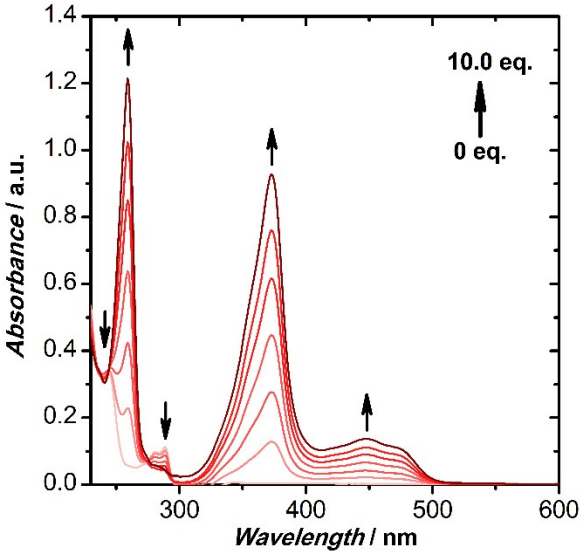

Figure S19a. UV-visible Al^{3+} titration into **X=O**. Initial spectrum in light red; final spectrum in dark red.

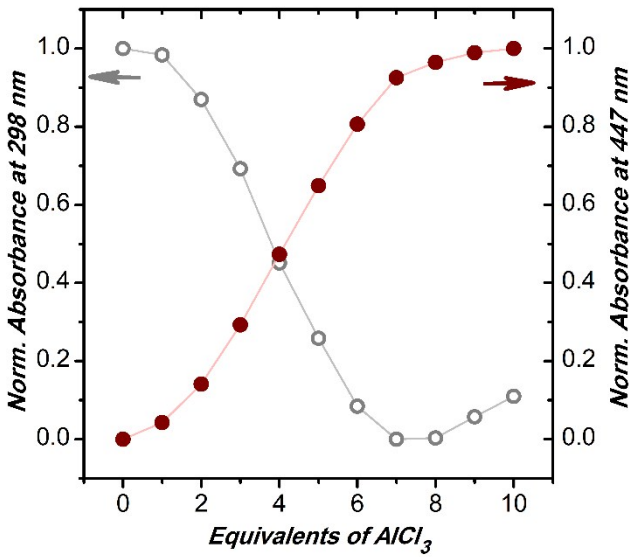

Figure S19b. Normalized absorbance for **X=O** (grey, open) and **[X=O]**$^+$ (red, closed) as a function of titrated equivalents of Al^{3+}.

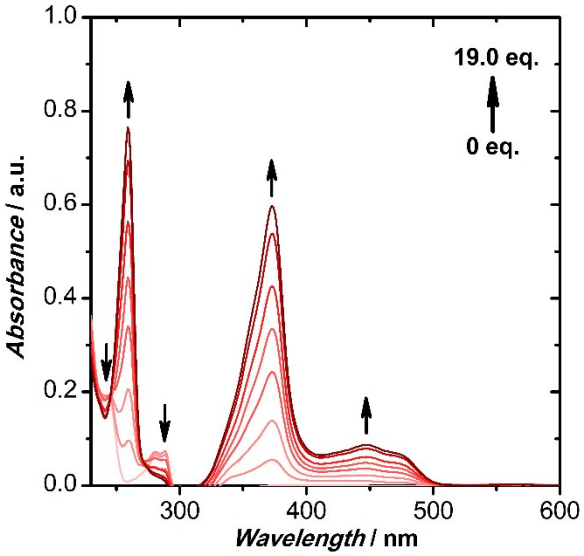

Figure S20a. UV-visible In^{3+} titration into **X=O**. Initial spectrum in light red; final spectrum in dark red.

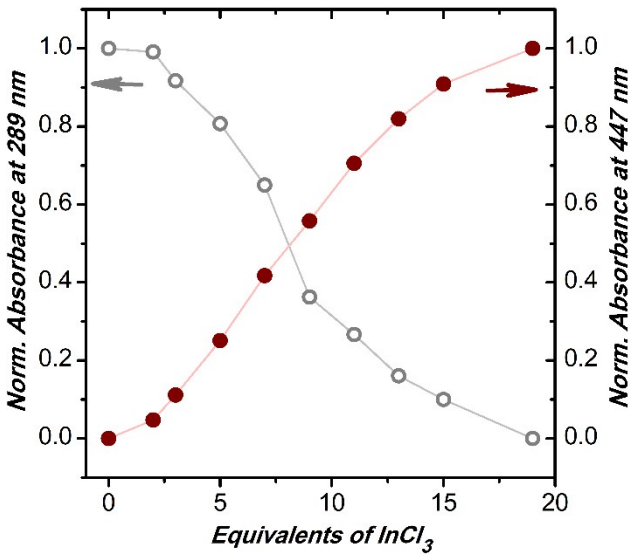

Figure S20b. Normalized absorbance for **X=O** (grey, open) and **[X=O]**$^+$ (red, closed) as a function of titrated equivalents of In^{3+}.

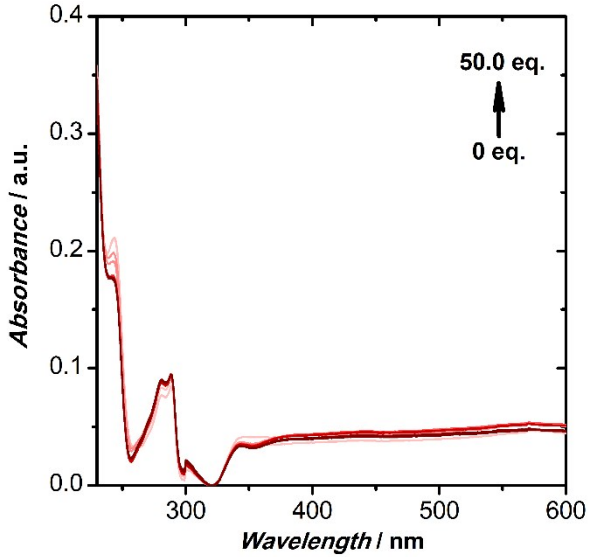

Figure S21. UV-visible Zn^{2+} titration into **X=O**. Initial spectrum in light red; final spectrum in dark red. Feature from 300-350 nm is a lamp artifact, consequence of lamp changeover at 310 nm instead of recommended 350 nm.

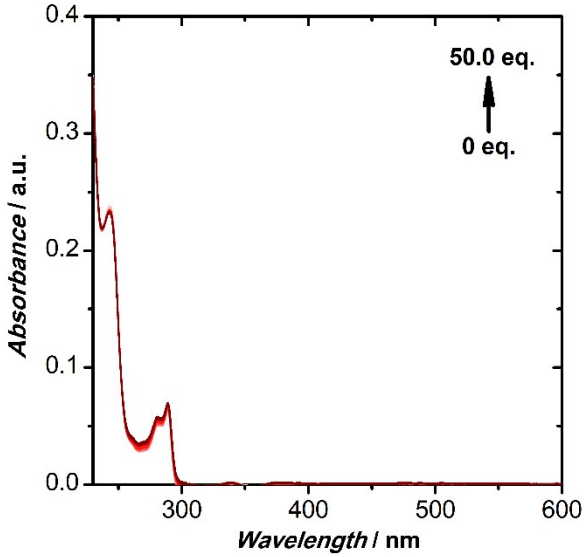

Figure S22. UV-visible Li^{+} titration into **X=O**. Initial spectrum in light red; final spectrum in dark red.

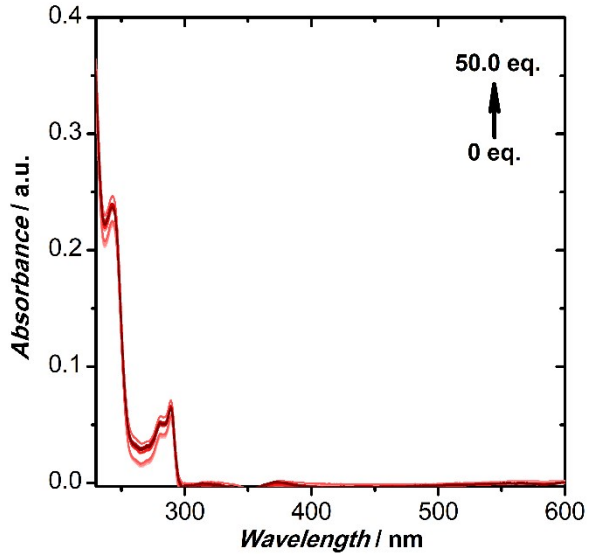

Figure S23. UV-visible Na^{+} titration into **X=O**. Initial spectrum in light red; final spectrum in dark red.

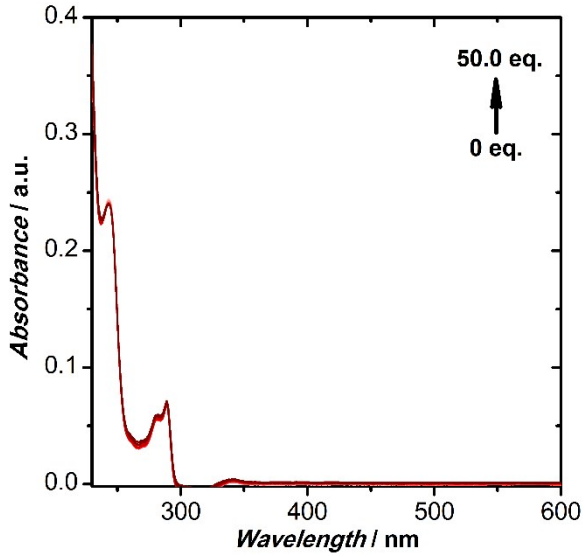

Figure S24. UV-visible TBACl titration into **X=O**. Initial spectrum in light red; final spectrum in dark red.

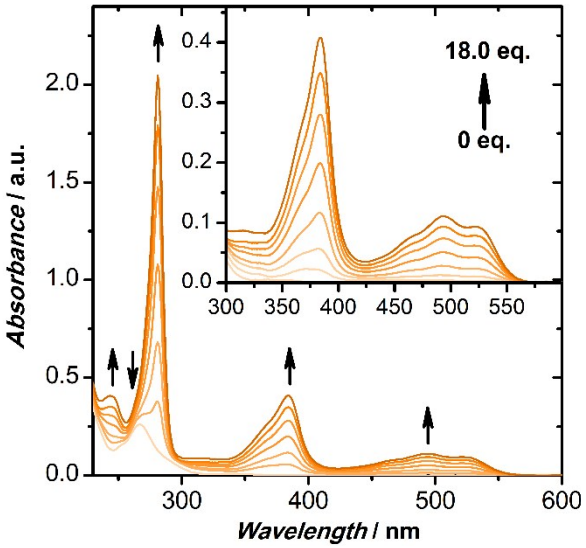

Figure S25a. UV-visible Al^{3+} titration into **X=S**. Initial spectrum in light orange; final spectrum in dark orange.

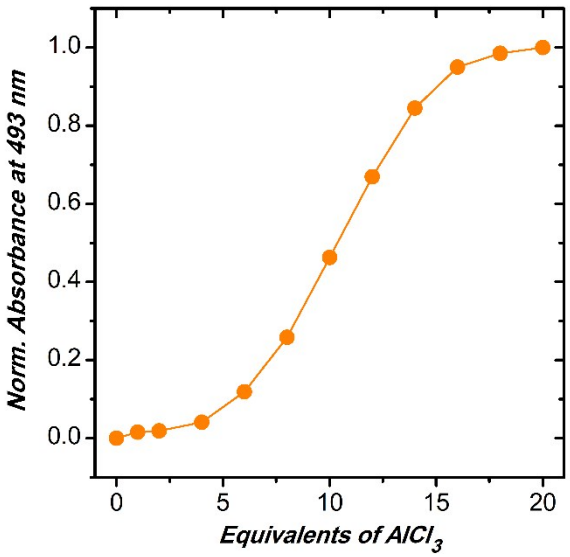

Figure S25b. Normalized absorbance for **[X=S]**$^{+}$ (orange, closed) as a function of titrated equivalents of Al^{3+}.

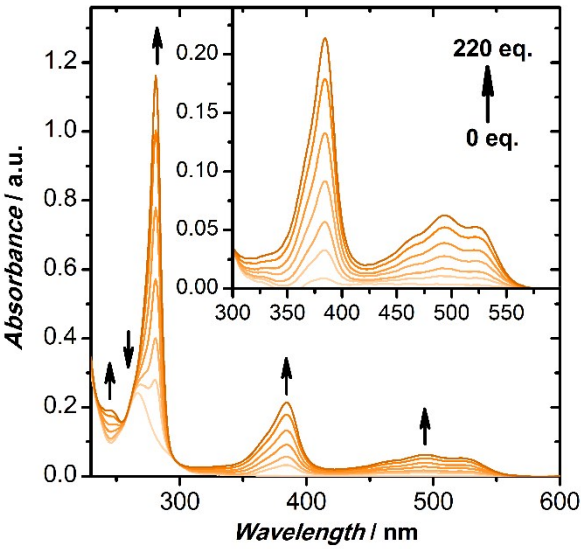

Figure S26a. UV-visible In^{3+} titration into **X=S**. Initial spectrum in light orange; final spectrum in dark orange.

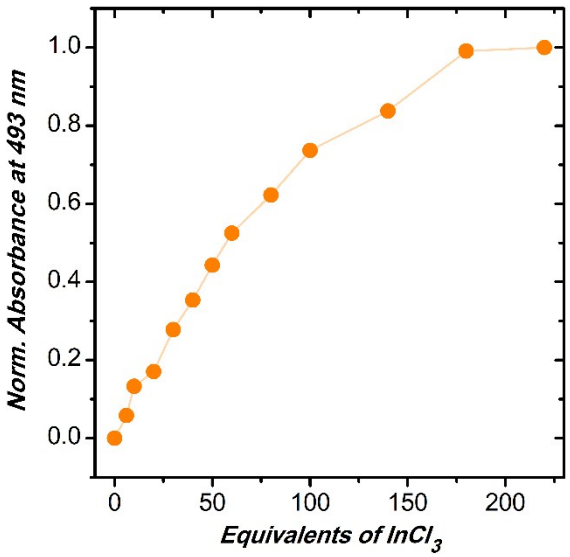

Figure S26b. Normalized absorbance for **[X=S]**$^{+}$ (orange, closed) as a function of titrated equivalents of In^{3+}.

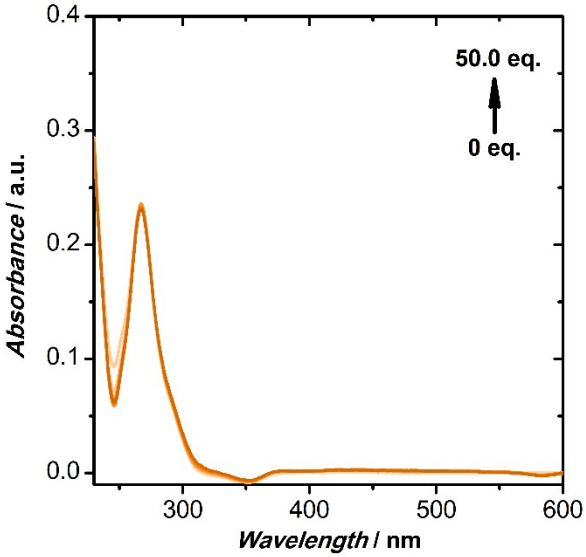

Figure S27. UV-visible Zn^{2+} titration into **X=S**. Initial spectrum in light orange; final spectrum in dark orange.

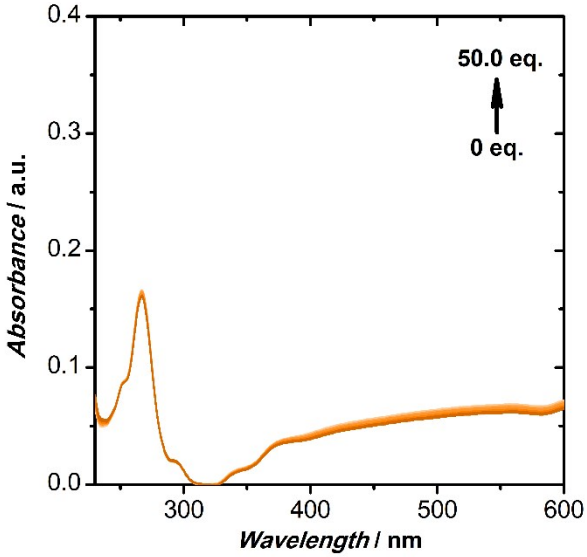

Figure S28. UV-visible Li^{+} titration into **X=S**. Feature from 300-350 nm is a lamp artifact, consequence of lamp changeover at 310 nm instead of recommended 350 nm. Initial spectrum in light orange; final spectrum in dark orange.

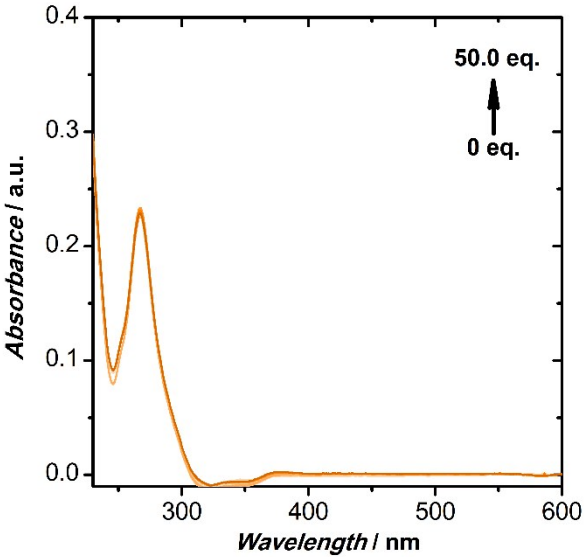

Figure S29. UV-visible Na^{+} titration into **X=S**. Initial spectrum in light orange; final spectrum in dark orange.

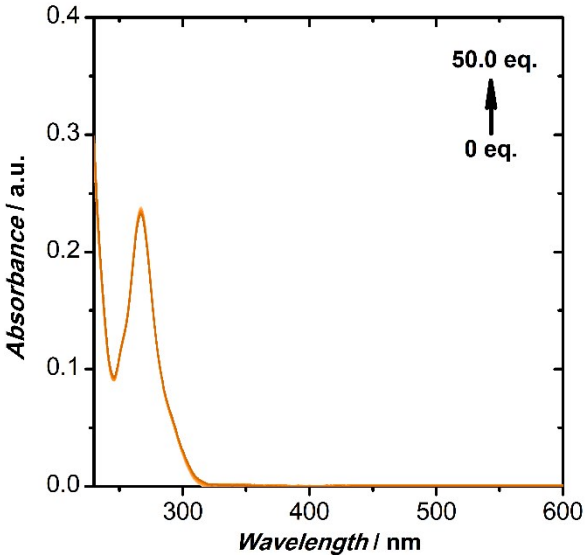

Figure S30. UV-visible TBACl titration into **X=S**. Initial spectrum in light orange; final spectrum in dark orange.

Table S3. Isosbestic Point Data

	Isosbestic Points (nm)
[X=NCH$_3$]OTf	233, 269, 325
[X=O]OTf	236, 245, 274, 295
[X=S]OTf	—[a]

[a] No isosbestic points are visible due to the proximity of the UV bands for **X=S** and **[X=S]$^+$**

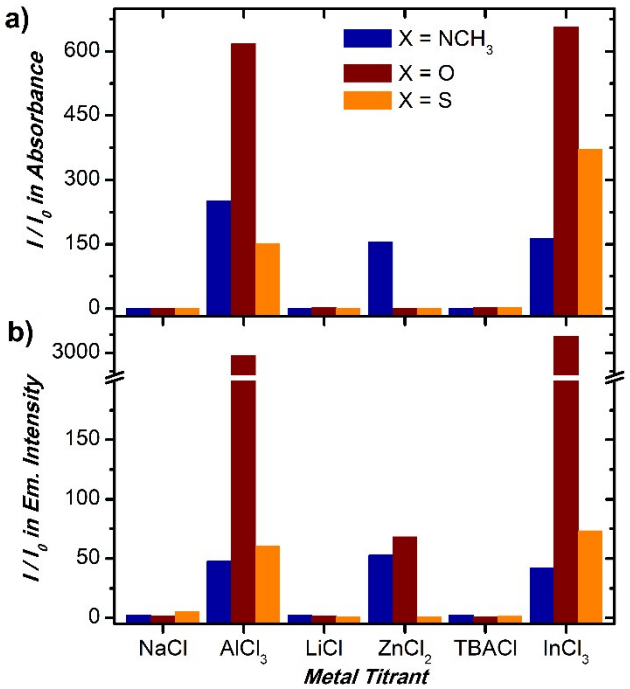

Figure S31. Metal cation-responsivity plot of (a) I/I_0 in absorbance at 424 nm (**X=NCH$_3$**), 447 (**X=O**) and 493 (**X=S**) following titrations with metal cations. (b) The analogous plot for increase in emission at 500 nm (**X=NCH$_3$**), 513 nm (**X=O**) and 563 nm (**X=S**).

Section 6 Emission Spectroscopic Titrations with Metal Cations

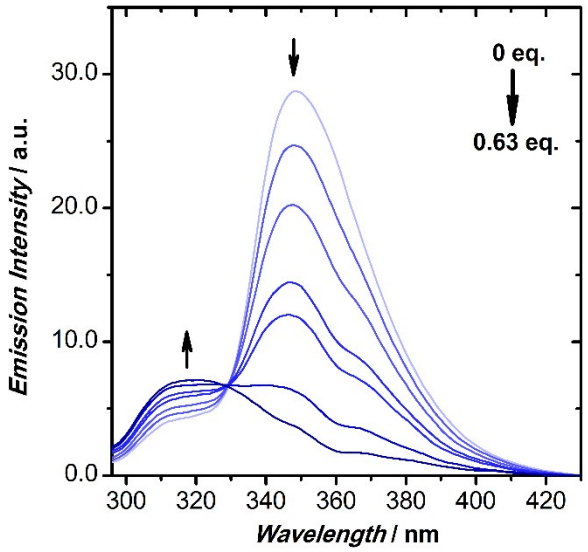

Figure S32a. Emission Al^{3+} titration into **X=NCH$_3$**, exciting at 286 nm. Initial spectrum in light blue; final spectrum in dark blue.

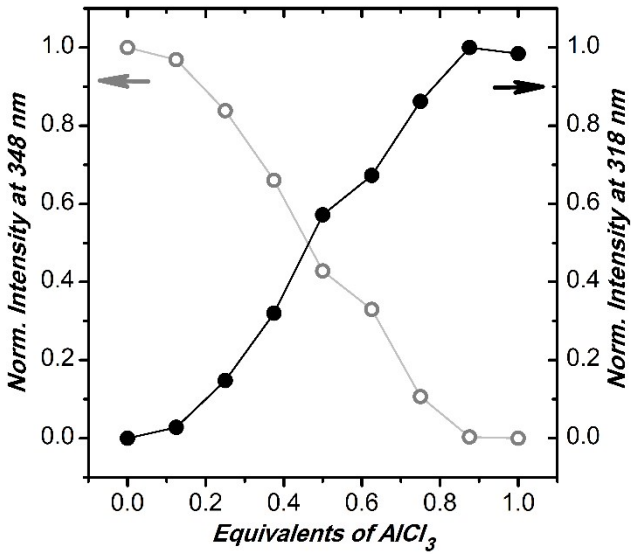

Figure S32b. Normalized emission for at 348 nm (grey, open) and 318 nm (black, closed) as a function of titrated equivalents of Al^{3+}.

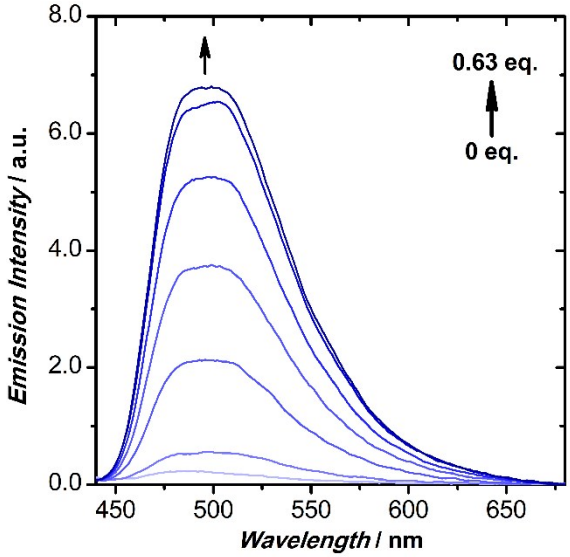

Figure S33a. Emission Al^{3+} titration into **X=NCH$_3$**, exciting at 361 nm. Initial spectrum in light blue; final spectrum in dark blue.

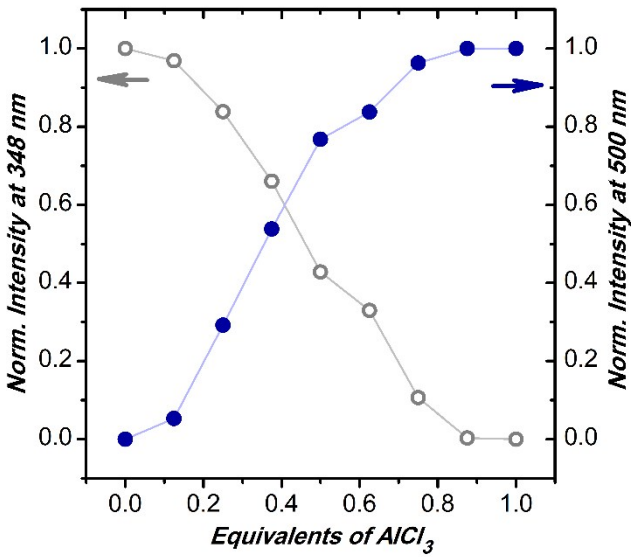

Figure S33b. Normalized emission for **X=NCH$_3$** (grey, open) and **[X=NCH$_3$]$^+$** (blue, closed) as a function of titrated equivalents of Al^{3+}.

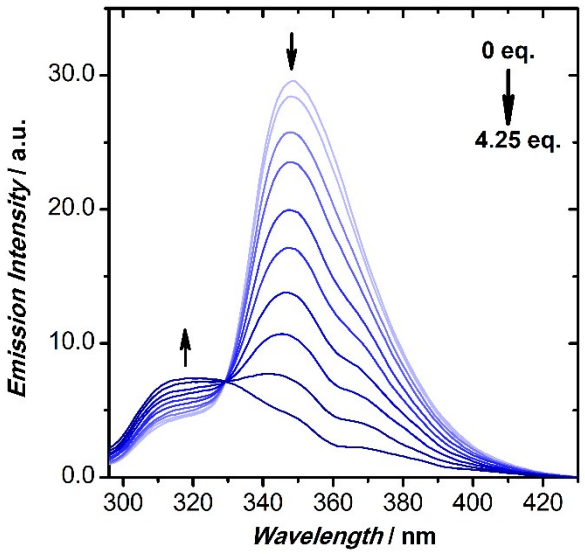

Figure S34a. Emission In^{3+} titration into **X=NCH$_3$**, exciting at 286 nm. Initial spectrum in light blue; final spectrum in dark blue.

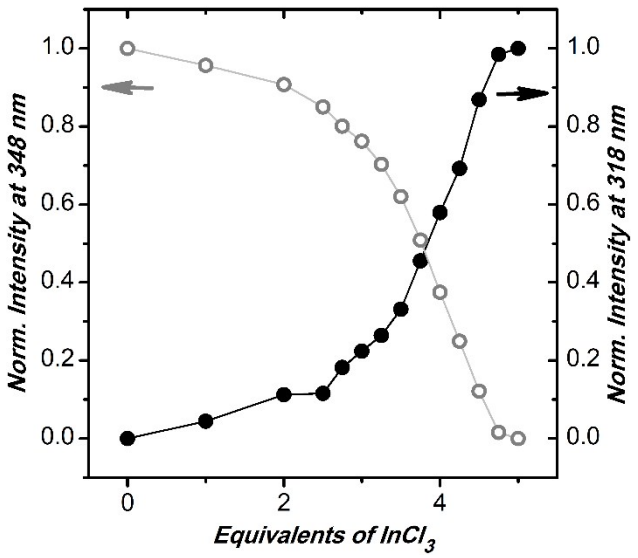

Figure S34b. Normalized emission for at 348 nm (grey, open) and 318 nm (black, closed) as a function of titrated equivalents of In^{3+}.

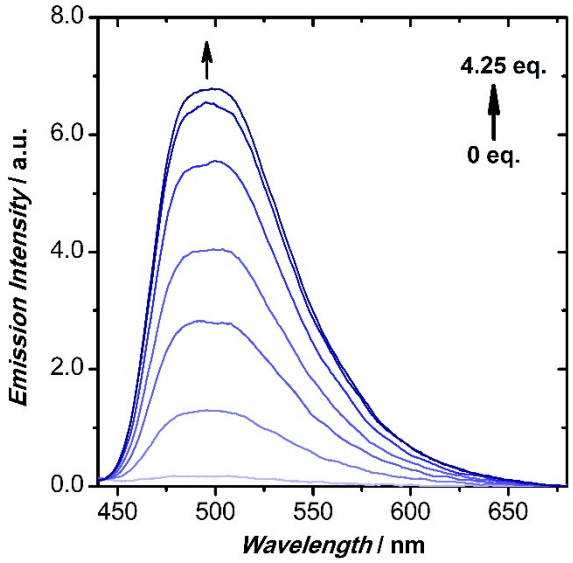

Figure S35a. Emission In^{3+} titration into **X=NCH$_3$**, exciting at 361 nm. Initial spectrum in light blue; final spectrum in dark blue.

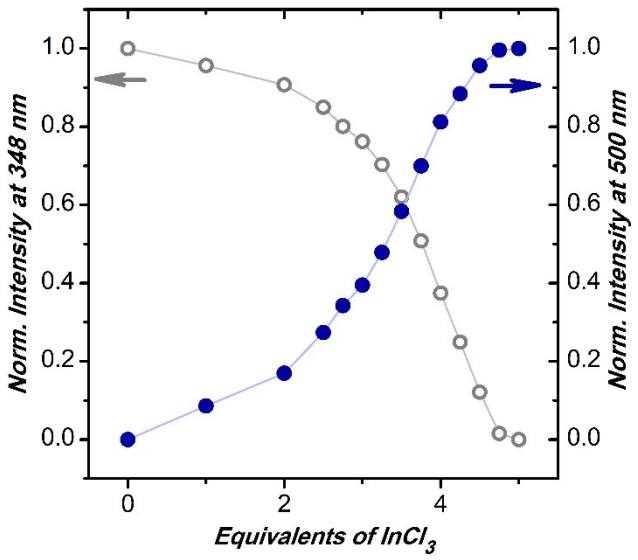

Figure S35b. Normalized emission for **X=NCH$_3$** (grey, open) and **[X=NCH$_3$]$^+$** (blue, closed) as a function of titrated equivalents of In^{3+}.

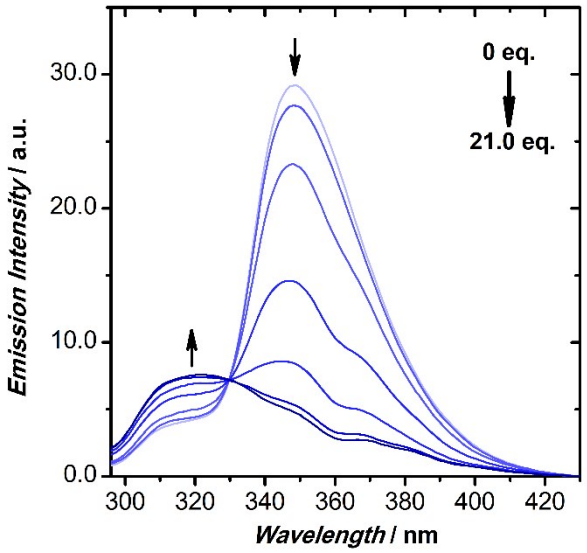

Figure S36a. Emission Zn^{2+} titration into **X=NCH$_3$**, exciting at 286 nm. Initial spectrum in light blue; final spectrum in dark blue.

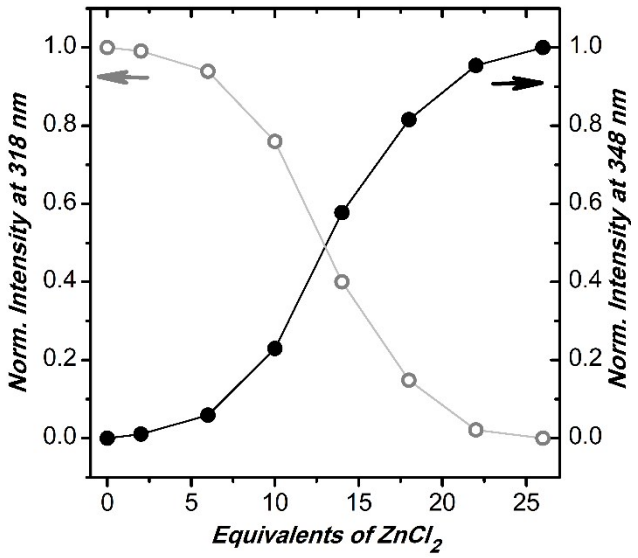

Figure S36b. Normalized emission for at 348 nm (grey, open) and 318 nm (black, closed) as a function of titrated equivalents of Zn^{2+}.

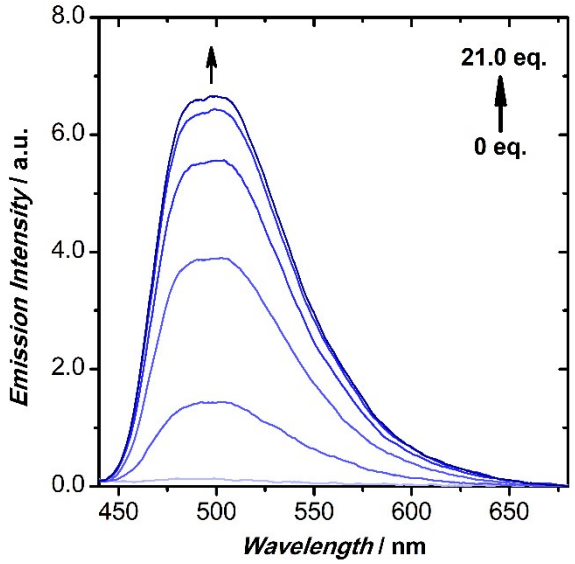

Figure S37a. Emission Zn^{2+} titration into **X=NCH$_3$**, exciting at 361 nm. Initial spectrum in light blue; final spectrum in dark blue.

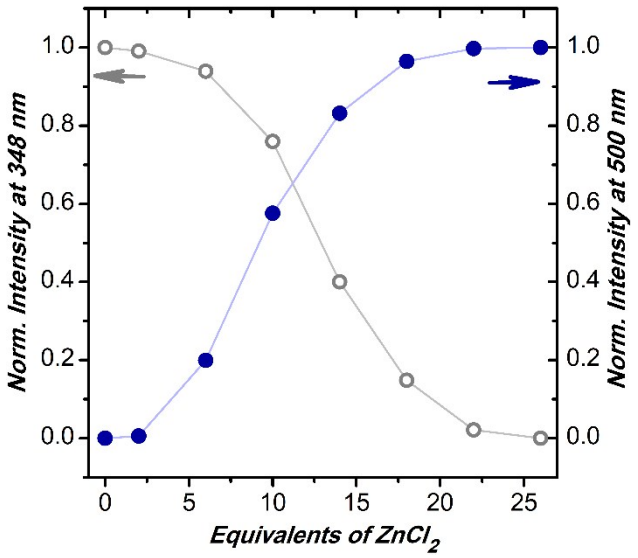

Figure S37b. Normalized emission for **X=NCH$_3$** (grey, open) and **[X=NCH$_3$]$^+$** (blue, closed) as a function of titrated equivalents of Zn^{2+}.

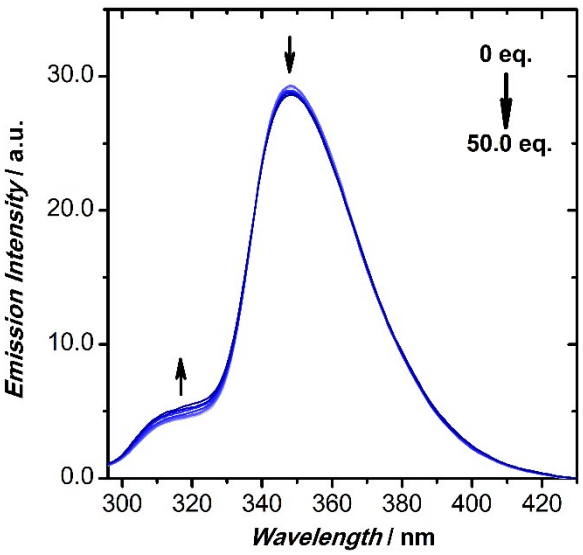

Figure S38. Emission Li^+ titration into **X=NCH$_3$**, exciting at 286 nm. Initial spectrum in light blue; final spectrum in dark blue. Increase is due to additional water present, not Li^+ (Figure S43/S44).

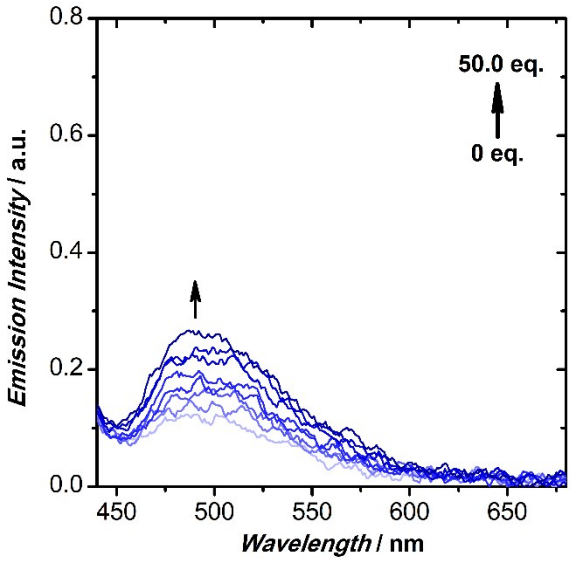

Figure S39. Emission Li^+ titration into **X=NCH$_3$**, exciting at 361 nm. Initial spectrum in light blue; final spectrum in dark blue. Increase is due to additional water present, not Li^+ (Figure S43/S44).

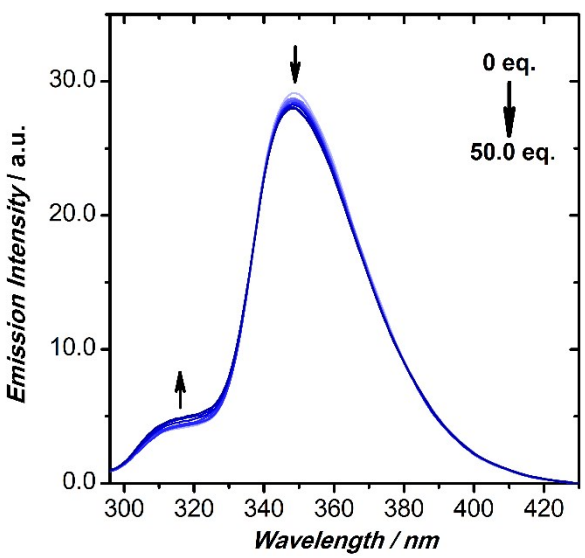

Figure S40. Emission Na^+ titration into **X=NCH$_3$**, exciting at 286 nm. Initial spectrum in light blue; final spectrum in dark blue. Increase is due to additional water present, not Na^+ (Figure S43/S44).

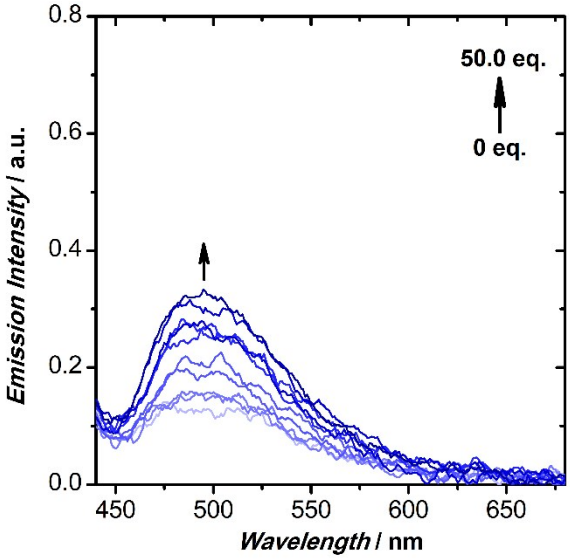

Figure S41. Emission Na^+ titration into **X=NCH$_3$**, exciting at 361 nm. Initial spectrum in light blue; final spectrum in dark blue. Increase is due to additional water present, not Na^+ (Figure S43/S44).

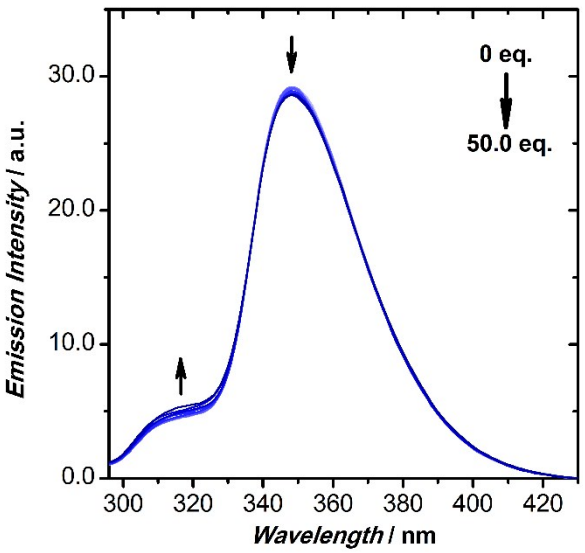

Figure S42. Emission TBACl titration into **X=NCH$_3$**, exciting at 286 nm. Initial spectrum in light blue; final spectrum in dark blue. Increase is due to additional water present, not TBACl (Figure S43/S44).

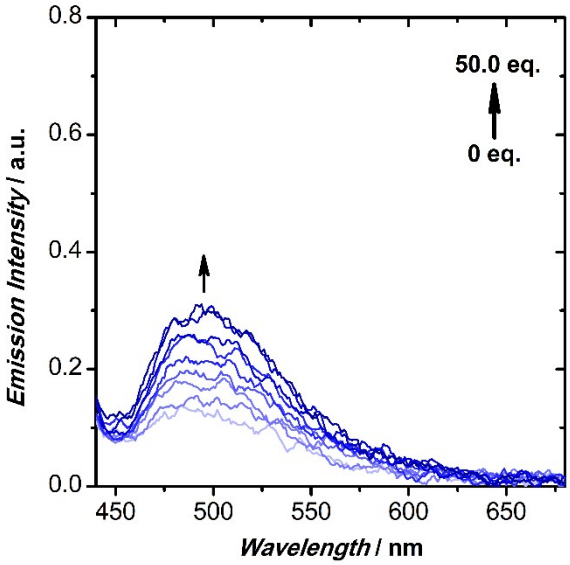

Figure S43. Emission TBACl titration into **X=NCH$_3$**, exciting at 361 nm. Initial spectrum in light blue; final spectrum in dark blue. Increase is due to additional water present, not TBACl (Figure S43/S44).

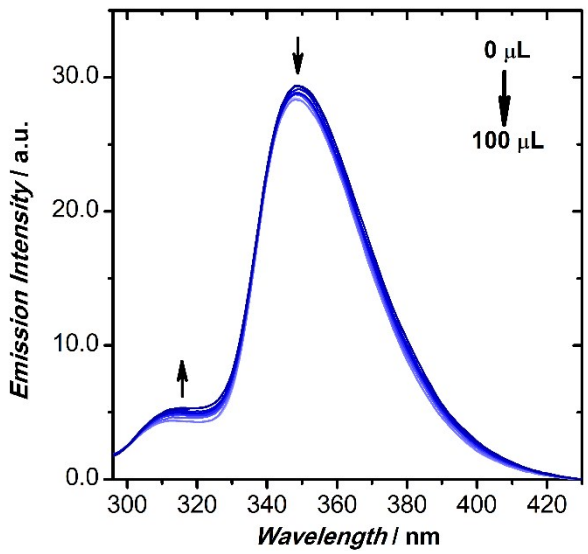

Figure S44. Emission CH_3CN titration into **X=NCH$_3$**, exciting at 286 nm. Initial spectrum in light blue; final spectrum in dark blue. This was done as a control to determine why the negative control TBACl exhibited slight turn-on behaviour. The decrease at 348 nm here is due to formation of **[X=NCH$_3$]$^+$** in the presence of trace water from dried CH_3CN.

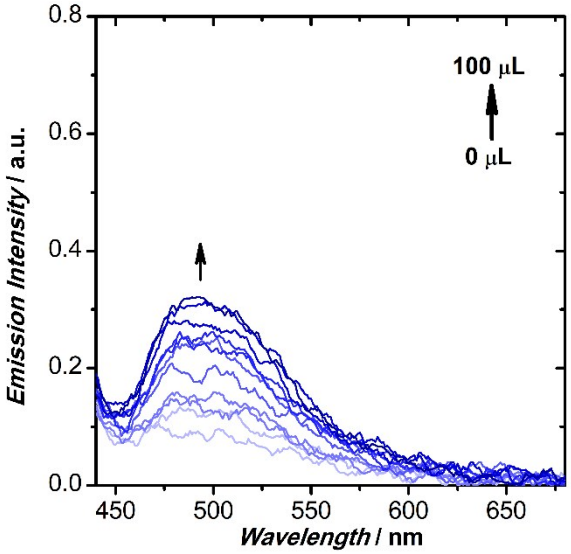

Figure S45. Emission 4L bottle-CH_3CN titration into **X=NCH$_3$**, exciting at 361 nm. Initial spectrum in light blue; final spectrum in dark blue. This was done as a control to determine why the negative control TBACl exhibited slight turn-on behaviour. The increase at 500 nm here is due to formation of **[X=NCH$_3$]$^+$** in the presence of water from non-dried 4L bottle-CH_3CN.

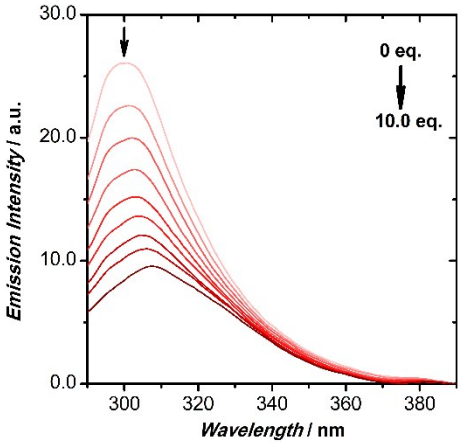

Figure S46a. Emission Al^{3+} titration into **X=O**, exciting at 280 nm. Initial spectrum in light red; final spectrum in dark red.

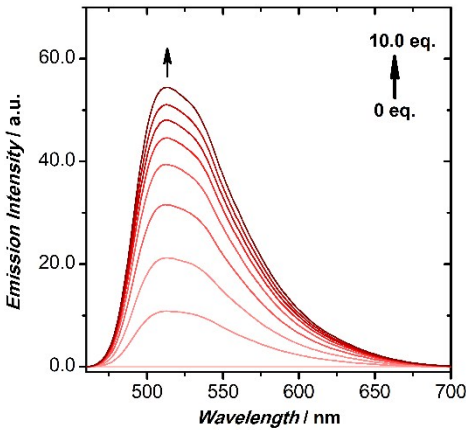

Figure S46b. Emission Al^{3+} titration into **X=O**, exciting at 373 nm. Initial spectrum in light red; final spectrum in dark red.

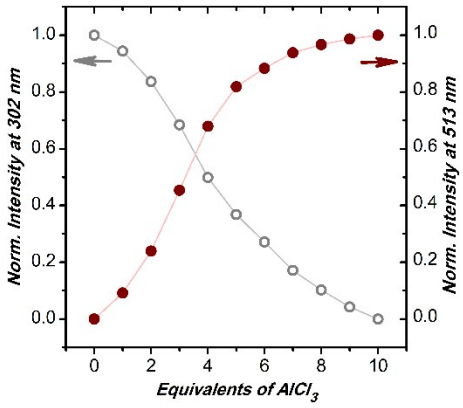

Figure S46c. Normalized emission for **X=O** (grey, open) and **[X=O]$^+$** (red, closed) as a function of titrated equivalents of Al^{3+}.

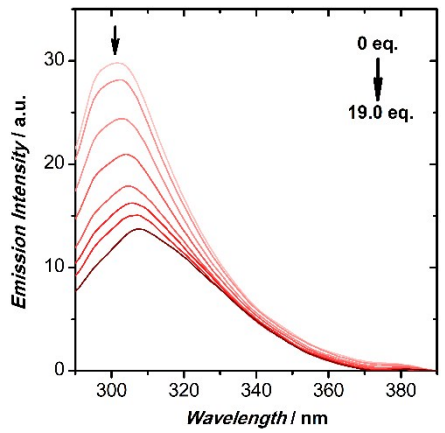

Figure S47a. Emission In^{3+} titration into **X=O**, exciting at 280 nm. Initial spectrum in light red; final spectrum in dark red.

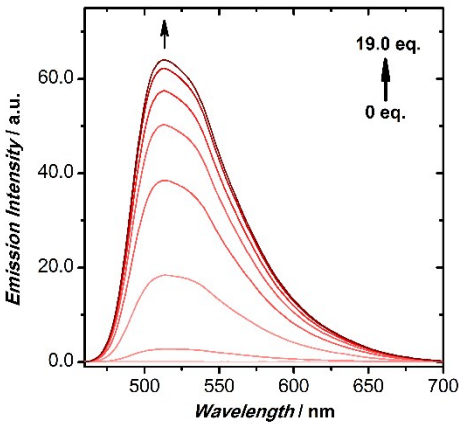

Figure S47b. Emission In^{3+} titration into **X=O**, exciting at 373 nm. Initial spectrum in light red; final spectrum in dark red.

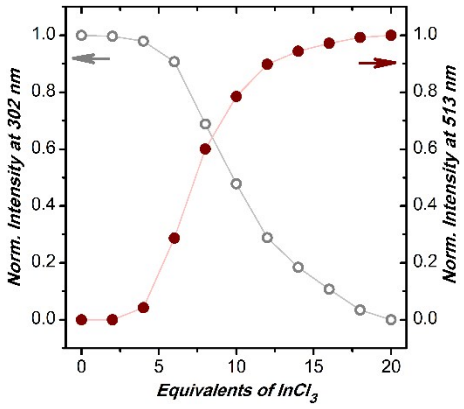

Figure S47c. Normalized emission for **X=O** (grey, open) and **[X=O]**$^{+}$ (red, closed) as a function of titrated equivalents of In^{3+}.

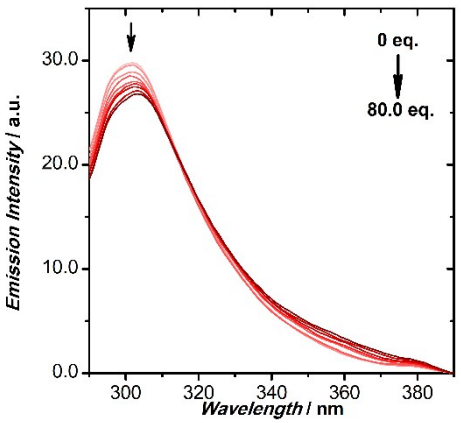

Figure S48a. Emission Zn^{2+} titration into **X=O**, exciting at 280 nm. Initial spectrum in light red; final spectrum in dark red.

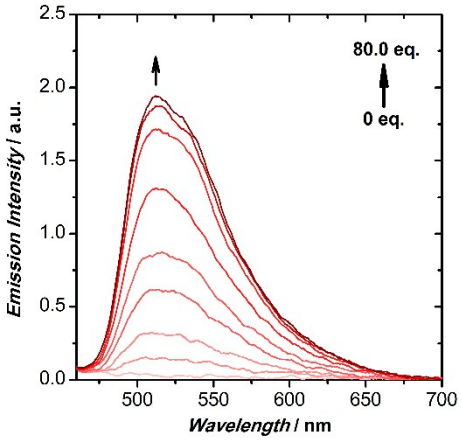

Figure S48b. Emission Zn^{2+} titration into **X=O**, exciting at 373 nm. Initial spectrum in light red; final spectrum in dark red.

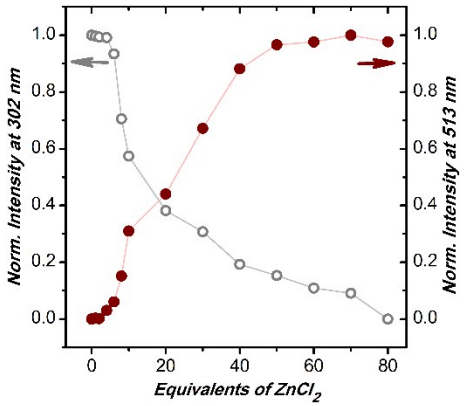

Figure S48c. Normalized emission for **X=O** (grey, open) and **[X=O]**$^{+}$ (red, closed) as a function of titrated equivalents of Zn^{2+}.

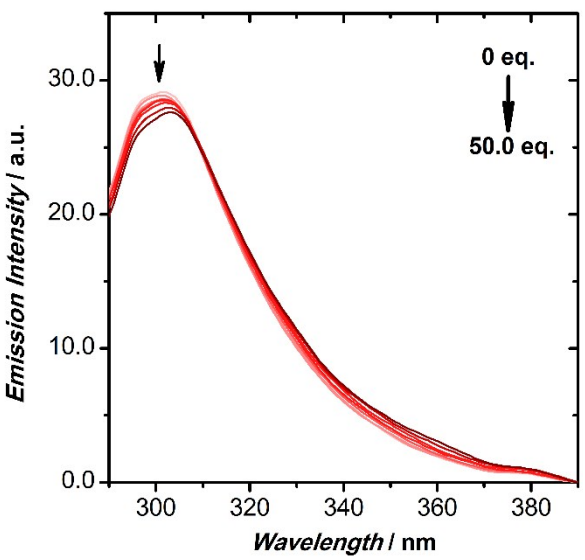

Figure S49. Emission Li^+ titration into **X=O**, exciting at 280 nm. Initial spectrum in light red; final spectrum in dark red.

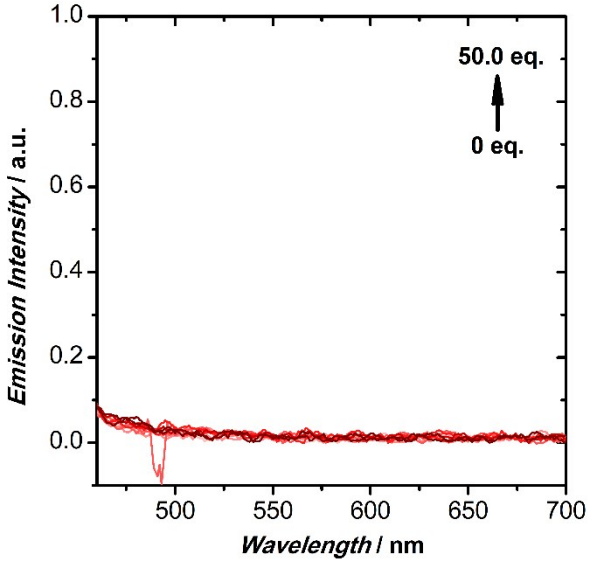

Figure S50. Emission Li^+ titration into **X=O**, exciting at 373 nm. Initial spectrum in light red; final spectrum in dark red.

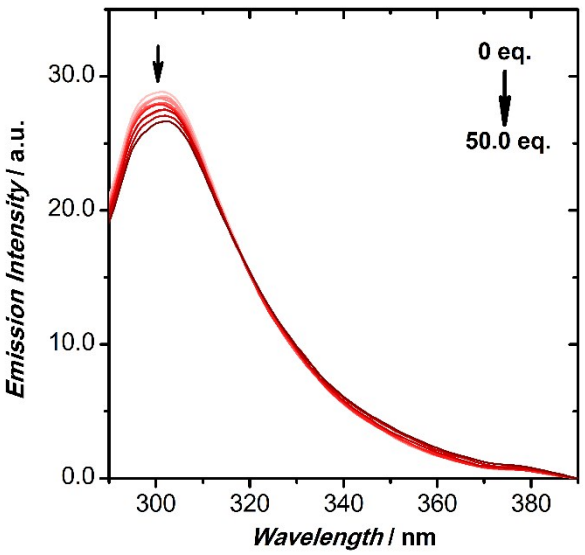

Figure S51. Emission Na^+ titration into **X=O**, exciting at 280 nm. Initial spectrum in light red; final spectrum in dark red.

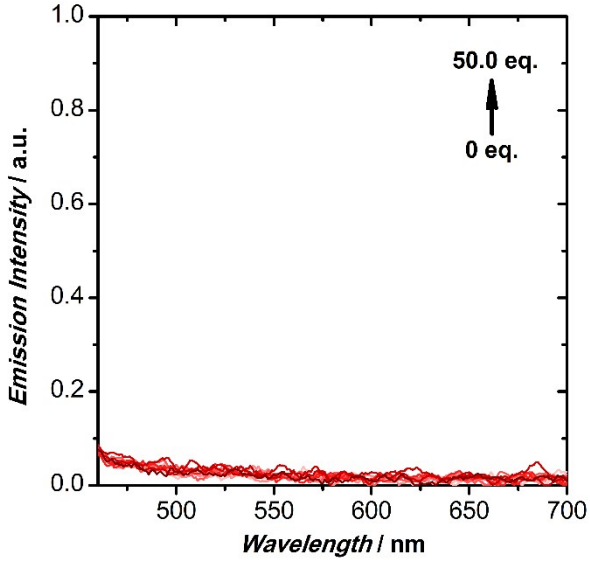

Figure S52. Emission Na^+ titration into **X=O**, exciting at 373 nm. Initial spectrum in light red; final spectrum in dark red.

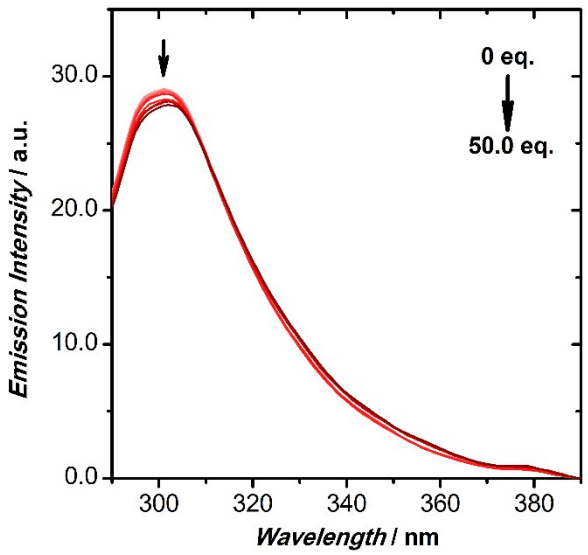

Figure S53. Emission TBACl titration into **X=O**, exciting at 280 nm. Initial spectrum in light red; final spectrum in dark red.

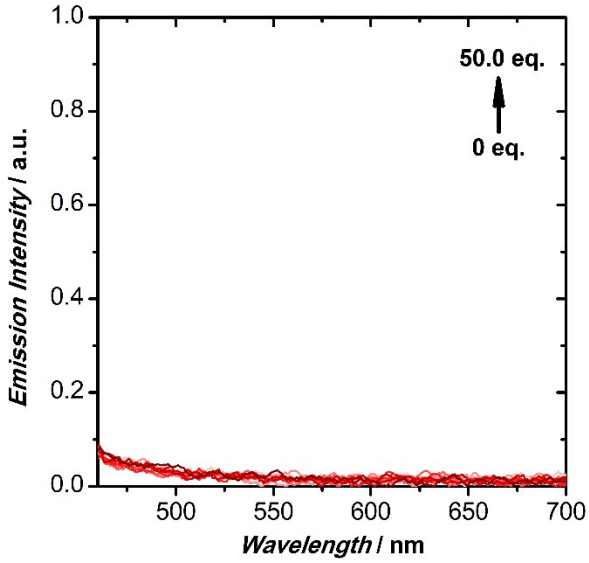

Figure S54. Emission TBACl titration into **X=O**, exciting at 373 nm. Initial spectrum in light red; final spectrum in dark red.

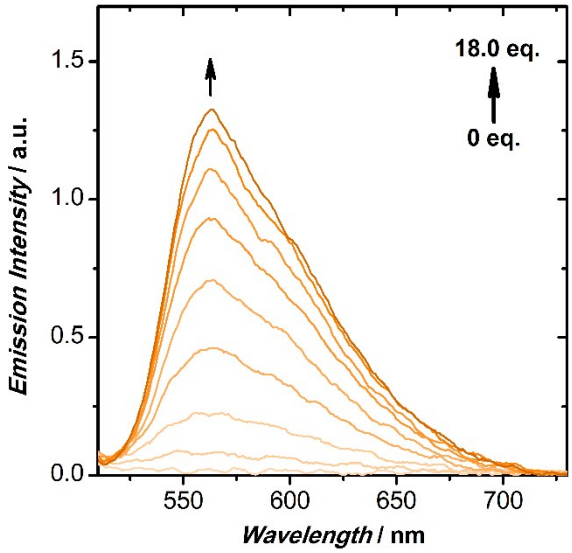

Figure S55a. Emission Al^{3+} titration into **X=S**, exciting at 384 nm. Initial spectrum in light orange; final spectrum in dark orange.

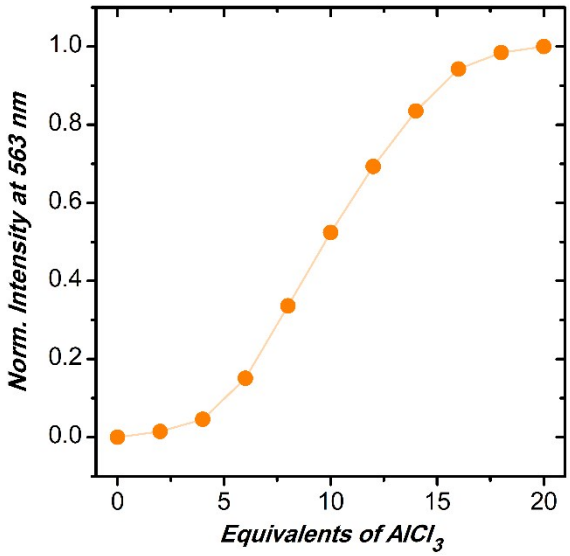

Figure S55b. Normalized emission for **[X=S]$^+$** (orange, closed) as a function of titrated equivalents of Al^{3+}.

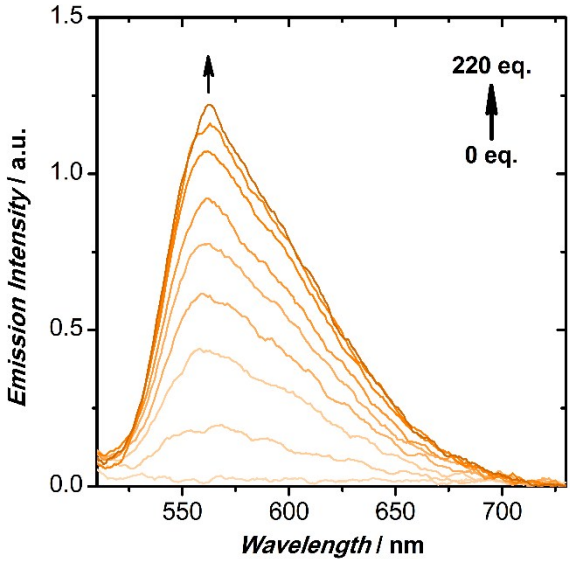

Figure S56a. Emission In^{3+} titration into **X=S**, exciting at 384 nm. Initial spectrum in light orange; final spectrum in dark orange.

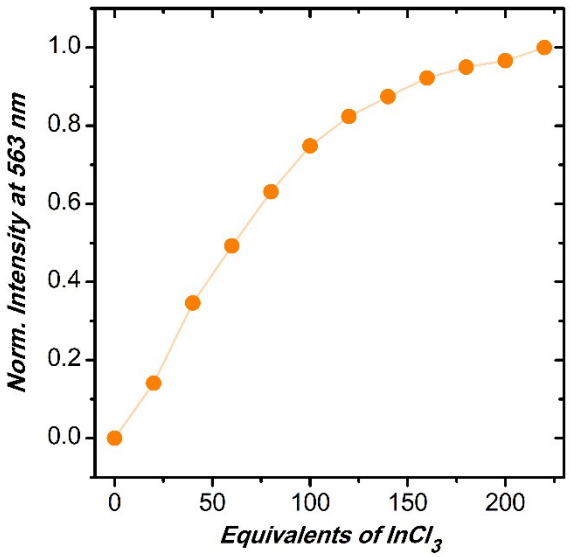

Figure S56b. Normalized emission for **[X=S]**$^{+}$ (orange, closed) as a function of titrated equivalents of In^{3+}.

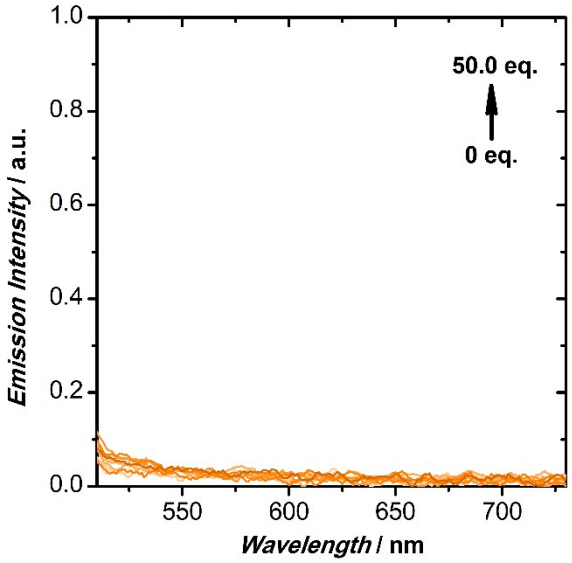

Figure S57. Emission Zn^{2+} titration into **X=S**, exciting at 384 nm. Initial spectrum in light orange; final spectrum in dark orange.

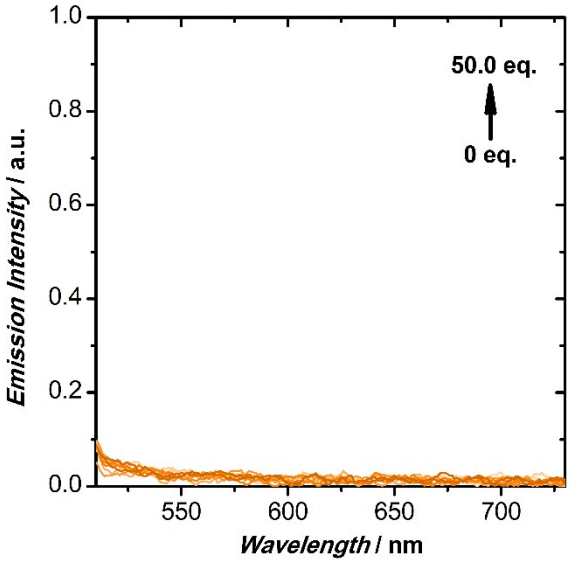

Figure S58. Emission Li^{+} titration into **X=S**, exciting at 384 nm. Initial spectrum in light orange; final spectrum in dark orange.

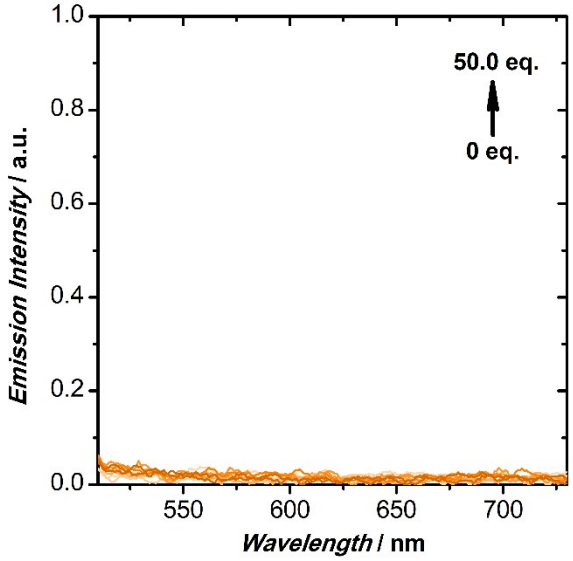

Figure S59. Emission Na^+ titration into **X=S**, exciting at 384 nm. Initial spectrum in light orange; final spectrum in dark orange.

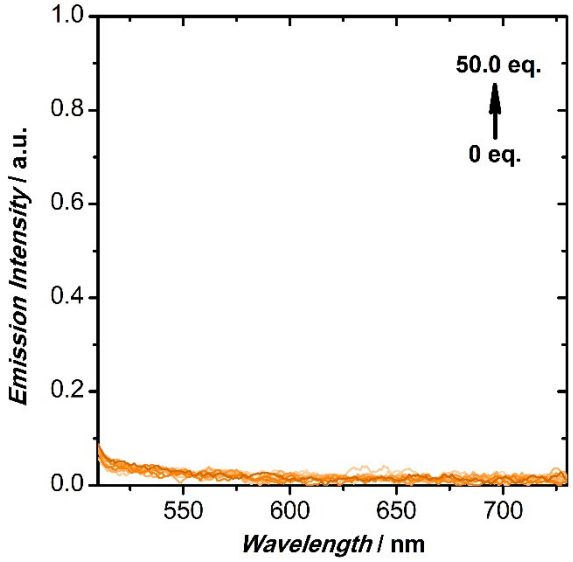

Figure S60. Emission TBACl titration into **X=S**, exciting at 384 nm. Initial spectrum in light orange; final spectrum in dark orange.

Section 7 UV-visible Spectroscopic Regeneration Titrations with $N(CH_3)_4OH$

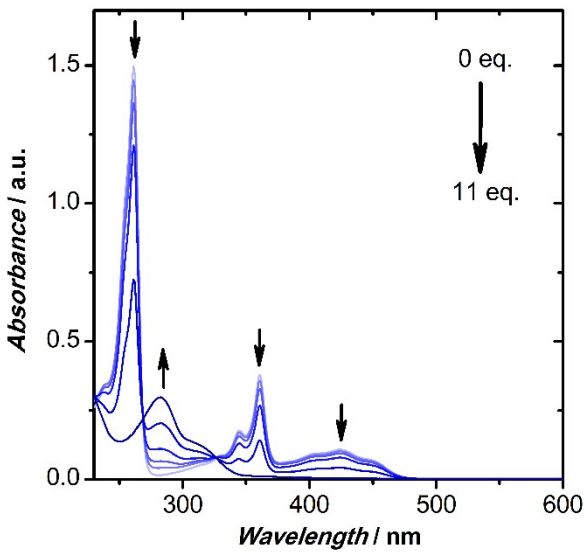

Figure S61. UV-visible $N(CH_3)_4OH$ titration into a solution containing **X=NCH$_3$** and 1 eq. of Al^{3+}. Initial spectrum in light blue; final spectrum in dark blue.

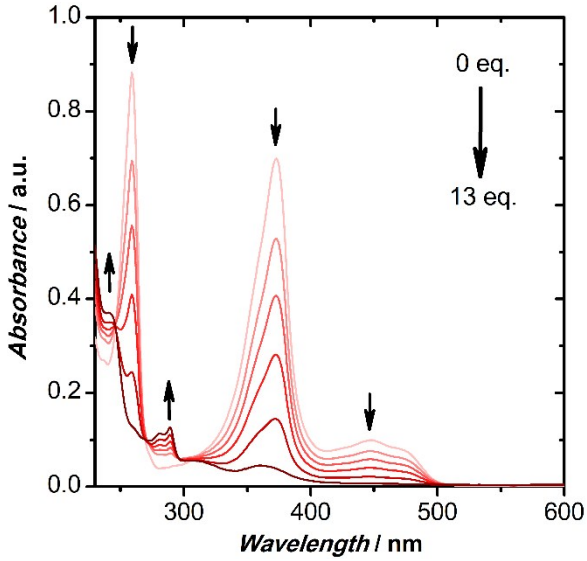

Figure S62. UV-visible $N(CH_3)_4OH$ titration into a solution containing **X=O** and 10 eq. of Al^{3+}. Initial spectrum in light red; final spectrum in dark red.

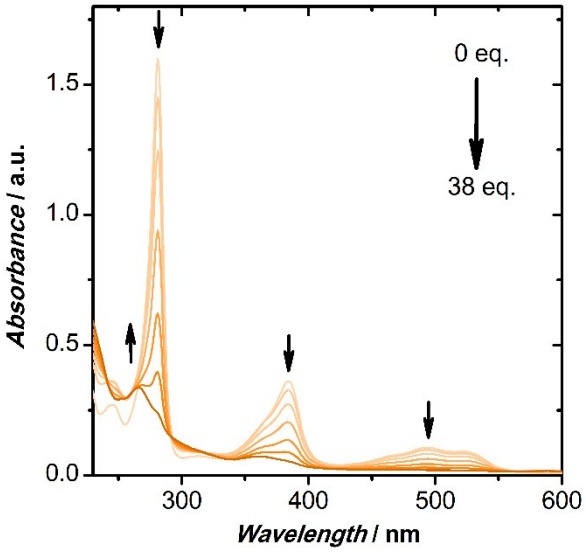

Figure S63. UV-visible $N(CH_3)_4OH$ titration into a solution containing **X=S** and 20 eq. of Al^{3+}. Initial spectrum in light orange; final spectrum in dark orange.